



Modulation of surface meteorological parameters by extratropical planetary-scale Rossby waves

K. Niranjan Kumar¹, D. V. Phanikumar^{1,2}, T. B. M. J. Ouarda^{1,3}, M. Rajeevan⁴, M. Naja², and K. K. Shukla^{2,5}

¹Institute Center for Water and Environment (iWater), Masdar Institute of Science and Technology, P.O. Box 54224, Abu Dhabi, United Arab Emirates

²Aryabhatta Research Institute of Observational Sciences, Nainital, India

³INRS-ETE, National Institute of Scientific Research, Québec (QC), G1K9A9, Canada

⁴Indian Institute of Tropical Meteorology, Dr. Homi Bhabha Road, Pashan, Pune, 411008, India

⁵Pt. Ravishankar Shukla University, Raipur, Chhattisgarh, 492010, India

Correspondence to: K. Niranjan Kumar (nirukin2003@gmail.com)

Received: 2 July 2015 – Revised: 26 November 2015 – Accepted: 30 December 2015 – Published: 25 January 2016

Abstract. This study examines the link between upper-tropospheric planetary-scale Rossby waves and surface meteorological parameters based on the observations made in association with the Ganges Valley Aerosol Experiment (GVAX) campaign at an extratropical site at Aryabhatta Research Institute of Observational Sciences, Nainital (29.45° N, 79.5° E) during November–December 2011. The spectral analysis of the tropospheric wind field from radiosonde measurements indicates a predominance power of around 8 days in the upper troposphere during the observational period. An analysis of the 200 hPa meridional wind ($v_{200\text{ hPa}}$) anomalies from the Modern-Era Retrospective Analysis for Research and Applications (MERRA) reanalysis shows distinct Rossby-wave-like structures over a high-altitude site in the central Himalayan region. Furthermore, the spectral analysis of global $v_{200\text{ hPa}}$ anomalies indicates the Rossby waves are characterized by zonal wave number 6. The amplification of the Rossby wave packets over the site leads to persistent subtropical jet stream (STJ) patterns, which further affects the surface weather conditions. The propagating Rossby waves in the upper troposphere along with the undulations in the STJ create convergence and divergence regions in the mid-troposphere. Therefore, the surface meteorological parameters such as the relative humidity, wind speeds, and temperature are synchronized with the phase of the propagating Rossby waves. Moreover, the present study finds important implications for medium-range forecasting through the upper-level Rossby waves over the study region.

Keywords. Meteorology and atmospheric dynamics (waves and tides)

1 Introduction

The boreal extratropical winter climate is generally constituted by strong jets and large-amplitude quasi-stationary planetary-scale (Rossby) waves. The background flow dictates the propagation of Rossby waves, which are linked to the strong vorticity gradient around the tropopause in extratropics (e.g., Hoskins and Ambrizzi, 1993; Branstator, 2002; Schwierz et al., 2004b). Theoretical and observational studies along with idealized numerical experiments have indicated that topographically and diabatically generated vortex anomalies at upper and lower levels can serve as triggers for Rossby waves propagating into the extratropics (Sardeshmukh and Hoskins, 1988; Hoskins and Karoly, 1981; Schwierz et al., 2004a; Niranjan Kumar and Ouarda, 2014). Also, a significant role in the amplification of the waves is played by the diabatic processes as demonstrated in a previous case studies (Massacand et al., 2001). The most dominant periods of the stationary planetary-scale waves (Rossby normal modes) corresponding to intrinsic periods are 2, 5, 8.3, and 12.5 days (Forbes, 1995). Moreover, Rossby waves have been recognized as important features that can influence the predictability of midlatitude weather systems, which have a forecast capability of 1–2 weeks (Shapiro and Thorpe, 2004; Hoskins, 2006).

More recent work has examined the link between Rossby waves or Rossby wave breaking and high-impact weather events. For instance, Niranjan Kumar et al. (2015) linked the breaking Rossby waves to episodes of extreme precipitation over the Arabian Peninsula. It has been found that the precursor waves to these breaking Rossby waves can be tracked up to 8 days in advance over the peninsular region. Similarly, precursor Rossby wave trains leading to heavy precipitation over the European Alps have been identified up to 8 days in advance and as much as 10 days for a case of flooding in Germany (Grazzini and Van der Grijn, 2003; Martius et al., 2006; Grazzini, 2007). It is also worth mentioning here that Grazzini (2007) studied the performance of the European Center for Medium-Range Weather Forecasts (ECMWF) system for these heavy-precipitation events and found that the forecasts had a higher than average skill on synoptic scales. The association between the long-lived Rossby wave trains and/or Rossby wave breaking and intense European cyclones is found mainly in the recent studies (e.g., Wirth and Eichhorn, 2014; Górnara et al., 2014).

It is well known from previous reports that Rossby waves remain in coherent over many days under favorable atmospheric conditions. They also propagate over long distances and can contribute to teleconnecting remote regions of the atmosphere (Chang and Yu, 1999; Niranjan Kumar and Ouarda, 2014). For example, Chang and Yu (1999) have shown that during December–January–February in the Northern Hemisphere, the Rossby wave packets are most coherent along a band that extends from northern Africa through southern Asia (maximum coherence) into the Pacific storm track. Moreover, knowledge of the evolution of coherent Rossby waves is crucial for weather forecasting since they set the stage for weather systems to evolve. Furthermore, analyses of forecast errors of numerical weather prediction models have revealed a close link between the propagation of the error patterns and the propagation of upper-level Rossby waves (Davies and Didone, 2013; Grazzini, 2015). Therefore, the study of the characteristics of extratropical Rossby waves, such as propagation, breaking, and their organization, is imperative for understanding and forecasting regional and local weather.

A significant fraction of weather-related loss of life and property in the extratropical latitudes is associated with severe convection (Pielke and Klein, 2001; Fritsch and Carbone, 2004). During the 21st century, there are several types of extreme weather events (heat waves, droughts and heavy rainfall events) that the IPCC (2012) considers to be increasing and becoming more frequent, more widespread, and/or intense in most parts of the world. A large number of recent extreme weather events have occurred in many parts of the world (for more details, refer to Coumou and Rahmstorf, 2012). Furthermore, the extreme events increase approximately in proportion to the ratio of the climate warming trend and short-term variability (Rahmstorf and Coumou, 2011). In several cases, these extreme weather events are

connected on the synoptic-to-planetary-scale framework associated with upper-level Rossby waves (e.g., Petoukhov et al., 2013; Screen and Simmonds, 2014).

Recent reports have also concentrated on the extreme rainfall events that could have resulted in several damaging floods in India (Goswami et al., 2006; Rajeevan et al., 2008; Guhathakurta et al., 2011). One such example of recent floods due to a heavy rainfall event, occurred in the state of Uttarakhand in June 2013, affecting the lives of thousands of people (Joseph et al., 2015). The trend analysis of heavy rainfall events over the country indicates an increasing trend, especially in the northern parts of India (Sinha Ray and Srivastava, 2000). These devastating floods in Uttarakhand affected the tourism industry, which is the principal contributor to the state gross domestic product (GDP). In addition, the extreme rainfall events were also recorded in the states of Himachal Pradesh and Jammu and Kashmir (Nibanupudi et al., 2015).

Thus, the state of Uttarakhand situated in the Indian Himalayan region is known to face disastrous climatic hazard events like floods and landslides. In order to improve prediction of the high-impact weather in this region, it is also necessary to have knowledge of the global-to-regional influences on the evolution and predictability of high-impact weather. Furthermore, knowledge is still lacking on the characteristics of long waves that have a significant influence on background flow and the creation of flow patterns conducive to the development of heavy rainfall events. Therefore, the presence of synoptic features in the lower stratosphere along with the complex topography may have significant influence on the evolution of extreme weather events over the region. However, to date, only limited studies exist describing the links between synoptic-scale tropospheric activity in the region and variability in the lower stratosphere.

Hence, the work presented here describes the observations at an extratropical site at Aryabhatta Research Institute of Observational Sciences (ARIES), Nainital (29.45° N, 79.5° E; 1958 m a.m.s.l.), located in the state of Uttarakhand. Over this site, a strong link has been found between the surface meteorological parameters and propagating upper-level Rossby waves. The surface meteorological observations along with radiosondes launched in association with the Ganges Valley Aerosol Experiment (GVAX) campaign during November–December 2011 offered a unique opportunity to better understand the link between the upper troposphere and surface weather. The following Sects. 2, 3, and 4 elaborate successively on the data used in this study and on the results and discuss them. Section 5 summarizes and concludes the present work.

2 Data description

The data were acquired through the measurements conducted at ARIES, Nainital, about 300 km northeast of New Delhi, India, during the GVAX campaign. GVAX was a re-

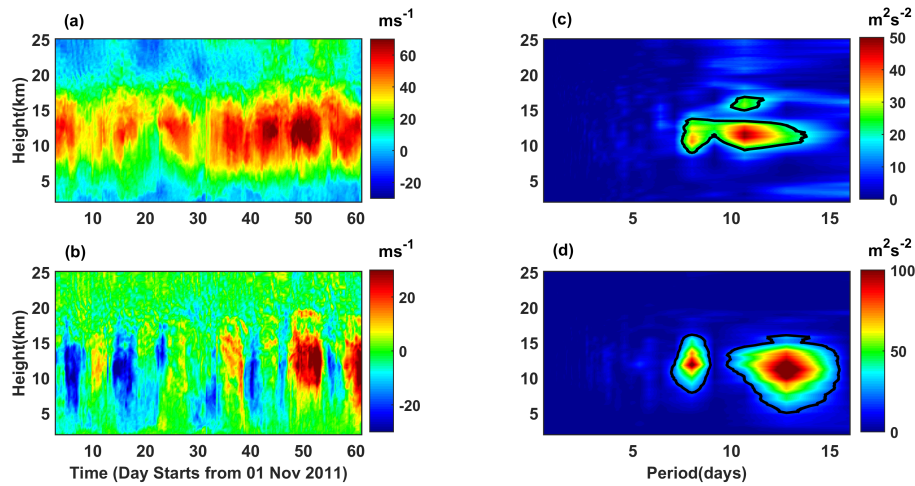


Figure 1. Zonal (**a**) and meridional (**b**) wind velocities measured by the radiosondes launched at 6-hourly intervals from an extratropical site at ARIES, Nainital (29.45° N, 79.5° E), between 1 November and 31 December 2011. The corresponding Fourier spectral amplitudes ($m^2 s^{-2}$) of zonal and meridional perturbations are shown in (**c**) and (**d**), respectively. The contours in (**c**) and (**d**) are significant at a 90 % confidence level.

sult of a joint research collaboration between the Indian Space Research Organization (ISRO), the Indian Institute of Science (IISc), ARIES, and the US Department of Energy (DOE). First, the Atmospheric Radiation Measurement Mobile Facility (AMF-1) was deployed at ARIES Observatory, Nanital, during June 2011–March 2012. In this study, the analysis is based on radiosondes (RS-92 Väisälä) launched every 6 h during November–December 2011. Pressure, humidity, wind, and temperature data were recorded every 2 s during ascent, giving a vertical resolution of roughly 10 m on average in the troposphere. We have also utilized the surface meteorological observations during the GVAX campaign. In situ sensors were used to measure the surface temperature, relative humidity (RH), and wind speed at a time interval of 1 min during the campaign period. For the present analysis, 1 min data are rearranged to obtain daily averages. The detailed technical report about the radiosonde and surface meteorological observation system (SMOS) can be found online (<http://www.arm.gov/publications/handbooks>).

To support the observations, we also make use of wind fields from Modern-Era Retrospective Analysis for Research and Applications (MERRA). MERRA is a reanalysis product generated by the National Aeronautics and Space Administration (NASA) Global Modeling and Assimilation Office (GMAO) using the Goddard Earth Observing System (GEOS) version 5.2.0 (Rienecker et al., 2011; <http://gmao.gsfc.nasa.gov/research/merra/>). MERRA has the advantage of incorporating information from a variety of recent in situ satellite data streams – for example, the observations from the Atmospheric Infrared Sounder (AIRS) and scatterometer-based wind retrievals. MERRA covers the period from 1979 to the present and continues to be updated with latency on the order of weeks. The model has a native

resolution of 72 layers in the vertical and $2/3^{\circ} \times 1/2^{\circ}$ in the horizontal. In addition to the 6-hourly 3-D analysis at the default spatial resolution, MERRA also provides 3-hourly 3-D diagnostics at $1.25^{\circ} \times 1.25^{\circ}$ resolution on 42 vertical levels, and this has been used in this study.

In addition, Tropical Rainfall Measuring Mission (TRMM) 3B42 (version 7) daily rainfall intensities are also used over the study region during the GVAX campaign period of November–December 2011. This product incorporates different types of sensors, namely microwave and infrared (Huffman et al., 2007, and references therein). TRMM-3B42 products were obtained at a spatial resolution of $0.25^{\circ} \times 0.25^{\circ}$ between 49.875° S and 49.875° N.

3 Results

Figure 1a and b portray the time–height cross section of horizontal winds from 1 November to 31 December 2011 based on 6-hourly radiosonde observations at an extratropical site of ARIES, Nainital. The zonal velocity is westerly through most of the troposphere and peaks at speeds in excess of 40 m s^{-1} in the subtropical jet stream (STJ) at an altitude of 12 km (Fig. 1a). The STJ is typically centered around 30° latitude at an altitude of about 12 km and is strongest in the winter season. Hence, Fig. 1a clearly depicts the strong STJ during winter over the observational site. The meridional wind field is displayed in Fig. 1b. It is apparent that the meridional winds depict alternating southerlies and northerlies in the upper troposphere. In the upper atmosphere, these anomalous patterns in meridional winds, termed Rossby waves, become quite prominent and associated with the jet stream at the top of the troposphere in extratropical latitudes.

Many studies have focused on the importance of upper-level tropospheric jets as waveguides for the observed low-frequency waves (e.g., Hoskins and Ambrizzi, 1993; Branstator, 2002). According to the waveguide theory, the propagating Rossby waves are confined to a narrow belt such as the jet region, and any disturbances along the jet stream may either trigger or enhance wave responses downstream (Hoskins and Ambrizzi, 1993; Branstator, 2002). To reveal the properties of the waves, a Fourier spectral analysis (FSA) of zonal and meridional winds at each height is performed. The FSA is a method by which a given times series is decomposed into several frequency components and this decomposition gives us an insight into physical mechanisms underlying the data series (Jenkins and Watts, 1968). Figure 1c and 1d show the results from the FSA. The FSA indicates strong amplitudes in the upper troposphere of around 8 days in both zonal and meridional wind components. However, the meridional spectrum depicts larger amplitudes relative to the zonal spectrum in the STJ region. This could be due to the fact that the eastward moving jet, comprising the ridges and troughs associated with Rossby waves, has a greater meridional component compared to the zonal component. Nevertheless, the predominance power in horizontal winds indicates that these are linked with upper-tropospheric Rossby waves with periods of around 8 days. Similar wave periods are also noted in previous reports (Forbes, 1995). It is also observed from Fig. 1c and d that the zonal and meridional spectrum peaks at different periods greater than 10 days. However, in this study we mainly focus on the spectral band of 6–10 days.

The vertical propagation characteristics of the Rossby waves are shown in Fig. 2. The height profiles of amplitude and phase of the selected harmonic component (around 8 days) are calculated by using the FSA method. The equations for the estimation of the magnitude and phase are described elsewhere in Smith (1997). The amplitude of Rossby waves shows its maximum in the upper troposphere. Afterwards it decreases with height in the troposphere, which further supports the result shown in Fig. 1b. However, it is interesting to note the phase propagation of Rossby waves as depicted in Fig. 2. The near-constant phase in the upper troposphere around 12 km indicates the source region of the Rossby wave activity. The notable feature is that the zonal velocity shows upward phase propagation of Rossby waves within the troposphere. In fact, the group velocity is orthogonal to the phase velocity, with upward phase propagation corresponding to the downward energy propagation. Fig. 2 suggests that wave energy flows downward into the troposphere from a source above in the upper troposphere. However, it is also true that the downward energy propagation occurs with a strong loss of amplitude in the troposphere as shown in Fig. 2. Due to the increase in mean atmospheric density with decreasing altitude, the amplitude of the waves decreases as they propagate downward in order to conserve wave energy. Nevertheless, it is interesting to see whether there is any effect of the upper-tropospheric Rossby waves

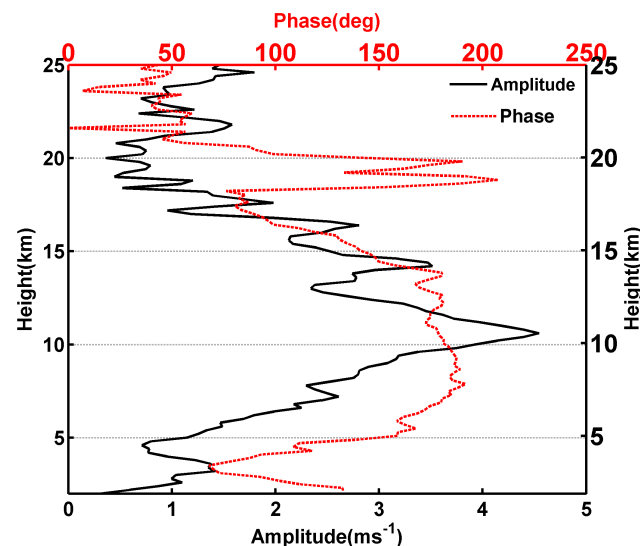


Figure 2. Height profiles of amplitude (m s^{-1}) and phase (deg) of Rossby waves (period ~ 8 days) in zonal winds observed by radiosonde measurements between 1 November and 31 December 2011.

on the surface meteorological parameters. This is because Rossby waves are long waves that play an important role in the formation of regions of divergence and convergence in the upper troposphere, further affecting the surface weather.

The surface meteorological observations during the GVAX campaign are shown in Fig. 3. For instance, Fig. 3 (left column) shows the time series of RH (a), pressure (b), temperature (c), and wind speed (d) from 1 November to 31 December 2011. RH, in particular, shows strong modulations, with a period of around 8 days. RH is an important parameter that explains the amount of moisture availability in the air, the formation of clouds, and rainfall. Therefore, the time series of rainfall acquired from the TRMM data averaged over a latitude-longitude grid box ($28\text{--}32^\circ \text{N}$, $78\text{--}82^\circ \text{E}$) is also overlaid along with RH in Fig. 3a. It is interesting to see that the rainfall time series oscillates with periods of between 6 and 10 days and closely follows the RH time series (Fig. 3a). This is more clearly seen in December 2011 than in November 2011 even though the percentage of RH is high. Nevertheless, the presence of moisture is not the only factor that determines rainfall as instability conditions associated with strong divergence and convergence at upper and lower levels, respectively, are also required. This will be further discussed in this section

The time series of surface pressure (Fig. 3b) also indicates the strong fluctuations in the 6–10-day period band. Furthermore, the time series of surface temperature is shown in Fig. 3c. It is known that RH is also dependent on air temperature. For instance, the combination of Fig. 3a and c indicates that an increase in temperature is reflected as a reduction in RH and vice versa. Also, the interrelationship be-

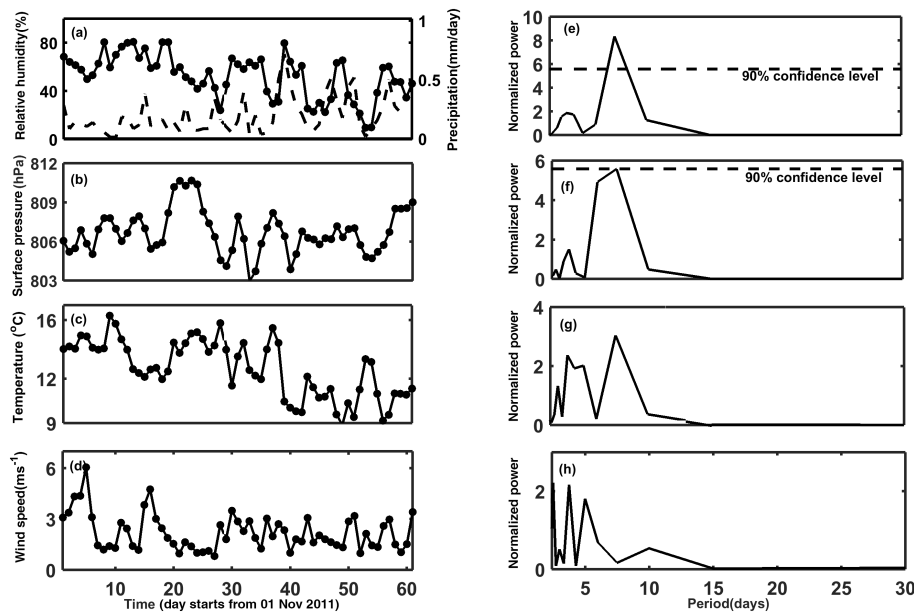


Figure 3. Left column: time series of surface meteorological parameters such as (a) RH, (b) pressure, (c) temperature, and (d) wind speed at ARIES, Nainital, from 1 November to 31 December 2011. The rainfall measured by the TRMM is also overlaid in (a) during the observational period (dashed line). Right column: the corresponding power spectrum estimated from Fourier analysis of (e) RH, (f) pressure, (g) temperature, and (h) wind speed perturbations.

tween the surface meteorological parameters has been well documented in several previous studies (e.g., Hardwick Jones et al., 2010 and references therein). The time series of surface wind speed during the observational period is shown in Fig. 3d. The highly dynamic nature of winds shows strong fluctuations compared with other surface parameters seen in Fig. 3.

Furthermore, confirmation regarding the modulations noticed in the time series of surface parameters is obtained through the FSA described previously (Fig. 3, right column). For instance, Fig. 3e shows the Fourier spectrum of RH. The horizontal dashed line indicates the statistical 90 % confidence level of the calculated spectral power. The RH spectrum shows a significant power for a period of around 8 days. It is the only period which is greater than the 90 % confidence level. The significance of the largest peak in the spectrum is computed based on the methodology described in Press et al. (1994). It is interesting to note here that both the upper-tropospheric Rossby waves and RH oscillate with the same periodicity. Also, the spectra of other surface parameters such as pressure (Fig. 3f), temperature (Fig. 3g), and wind speed (Fig. 3h) indicate the strong power between 6- and 10-day periods. However, the wind speed spectrum is slightly shifted to higher frequencies. This may be due to the Doppler shift effect in the presence of background surface winds. The spectra of temperature and wind speed below indicate the statistical 90 % confidence level (not shown in the plots), yet they also indicate that there undoubtedly is an ef-

fect of the upper-tropospheric Rossby waves on the surface meteorological fields.

In order to have a closer look at physical mechanisms through which propagating Rossby waves in the upper troposphere can influence surface weather, MERRA global reanalysis data are analyzed. For example, Fig. 4 shows the time–pressure cross section of RH overlaid with divergence contours over Nainital. The divergence (F) is computed using the function defined by

$$\nabla \cdot F = \frac{\partial u'}{\partial x} + \frac{\partial v'}{\partial y}, \quad (1)$$

where u' and v' are the filtered zonal and meridional amplitudes, respectively, in the 6- and 10-day period band. Figure 4a shows interesting features of a series of divergence–convergence patterns with time in the upper troposphere (above 400 hPa) in December 2011. Conversely, one can also note the convergence–divergence patterns in the lower troposphere below the 500 hPa pressure level. The strong upper-level divergence and convergence occur when deep troughs and ridges exist in the flow aloft. This will be discussed further in this section. Figure 4a shows that the strong upper-tropospheric divergence corresponds to lower-tropospheric convergence during 5–11 December 2011. The convergence in the lower levels results in an increase in RH in the troposphere below 200 hPa, while strong convergence in the upper troposphere during 12–15 December 2011 results in divergence below 500 hPa. Hence, there is less moisture available over the observational site. Similarly to Fig. 4a, Fig. 4b

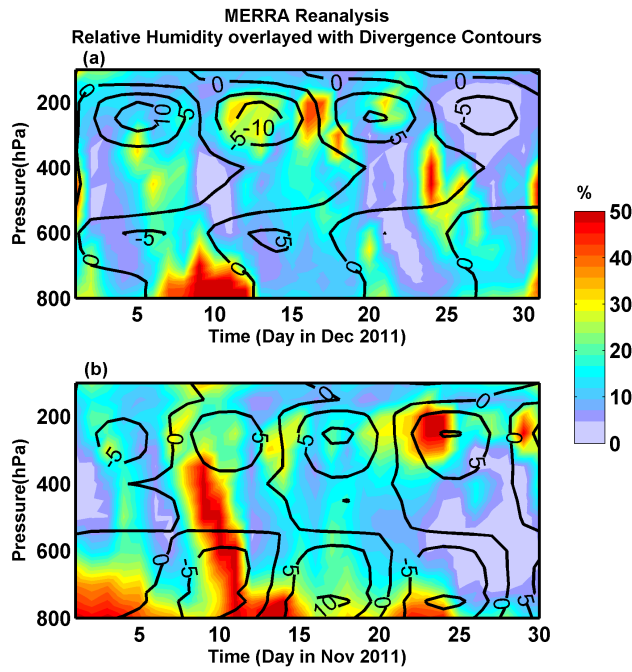


Figure 4. Panel (a): pressure (hPa)-versus-time contour plot of relative humidity (%) and overlaid divergence contours (in units of 10^{-6} s^{-1}) derived from MERRA reanalysis data (solid black lines) over the observational site between 1 and 31 December 2011. Panel (b): same as (a) but from 1 to 30 November 2011.

shows the time–pressure cross section of RH overlaid with divergence contours in November 2011. It may also be noted from Fig. 4b that the upper-tropospheric divergence leads to convergence at lower levels, especially in the first half of November 2011. However, the strength of the divergence at upper levels is comparatively less than the divergence values in Fig. 4a. This further supports the results in Fig. 3a where the rainfall in November 2011 is less compared to December 2011.

The vertical section of circulation seen in Fig. 4 indicates that the anomalous ascending motion in the troposphere appearing over the site is accompanied by anomalous upper-tropospheric divergence and lower-tropospheric convergence and vice versa. It is apparent that the convergence–divergence pattern seen in the upper troposphere (Fig. 4) also influences the surface meteorological parameters (Fig. 3). As an example, the anomalous subsidence in the lower troposphere due to strong convergence in the upper troposphere results in less RH and rainfall from 12 to 15 December 2011, which is evident from Fig. 3a. Likewise, the strong divergence in the upper troposphere results in increased RH and rainfall from 8 to 11 December 2011 (Fig. 3a). Hence, Figs. 3 and 4 signify that the upper-tropospheric divergence–convergence occurs in conjunction with the anomalous propagation of Rossby waves and further modulates the surface parameters

The location of the Rossby wave and the associated jet stream can explain the formation of convergence and divergence regions over the observational site. Hence, at this juncture it is interesting to see the spatial pattern of Rossby wave activity along with the latitudinal position of STJ. To show this, we utilize the MERRA meridional wind anomalies at the 200 hPa (hereafter abbreviated as $v_{200} \text{ hPa}$) along with the upper-tropospheric zonal velocity at 200 hPa pressure level ($u_{200} \text{ hPa}$). Figure 5a and b show $v_{200} \text{ hPa}$ anomalies and $u_{200} \text{ hPa}$ zonal velocities, respectively on 8 December 2011, whereas Fig. 5c and d highlight these parameters for 12 December 2011. The $v_{200} \text{ hPa}$ anomalies are obtained by applying a band-pass filter of between 6 and 10 days. The geographical location of the ARIES (indicated by the star) along with the position of the STJ are also shown in Fig. 5a and c. The location of the jet stream is obtained by taking the maximum wind velocity between the latitude band 20 and 45°N for all the longitudes. Note that the STJs do not pursue a latitudinal course at their respective positions but instead meander. In particular, the upper-tropospheric signature of a synoptic Rossby wave is evident as major lateral undulations of the jet stream (Fig. 5).

The curving of the jet stream poleward over the observational site on 8 December 2011 is clear from Fig. 5a and b. Air moving poleward in the upper atmosphere undergoes divergence. This is also supported by Fig. 4, since a strong divergence exists in the upper troposphere over the observational site on 8 December 2011. The upper-air divergence is compensated for by convergence in the lower troposphere (Fig. 4). By contrast, Fig. 5c and d show the jet stream swing towards the equator over the observational site on 12 December 2011. We can observe that as the jet stream enters a trough, it narrows and air converges into it. A strong convergence is also evident in Fig. 4 on 12 December 2011 at higher level and is compensated for by divergence in the lower troposphere. Hence, the undulations in the STJ connected with the upper-tropospheric Rossby waves are responsible for the observed modulations seen in surface meteorological parameters over the observational site of Manora Peak during the GVAX campaign in November–December 2011.

4 Discussion

The two key links observed in this study between the upper air and surface are Rossby waves and the subtropical jet. However, the Rossby waves and STJ commonly work in tandem providing vertical motions and influence the daily weather. Hence, the changes to airflow patterns around the extratropical latitudes and in the Northern Hemisphere seem to influence prolonged spells of extreme weather. For instance, the dynamical forcing associated with the propagating upper-tropospheric Rossby waves from the west Pacific played dominant role in initiating dry-spell conditions over the Great Plains region of the United States (Lyon and Dole,

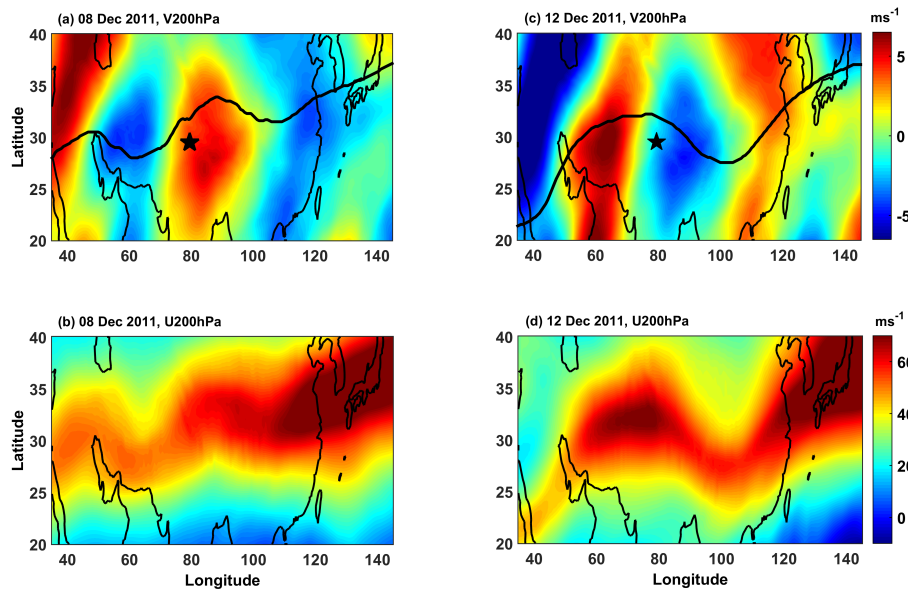


Figure 5. Meridional wind anomalies (a) at 200 hPa pressure level ($v_{200\text{hPa}}$) overlaid with the position of subtropical jet stream (thick solid black line) and zonal wind (b) at 200 hPa pressure level on 8 December 2011 obtained from MERRA reanalysis. (c) and (d) Same as (a) and (b) except on 12 December 2011. The location of ARIES, Nainital (29.45° N, 79.5° E), is also indicated by the star in (a) and (c).

1995; Chen and Newman, 1998). Furthermore, Schubert et al. (2011) showed the stationary Rossby waves account for more than 30% (60%) of the monthly mean precipitation (surface temperature) over many regions of extratropical land areas and at the same time that they are major players in the development of short-term climate extremes. In addition, Schubert et al. (2011) stressed that the current general circulation models do not simulate and predict the development of such Rossby waves. More recent studies have also reported that month-long periods of extreme weather are associated with anomalous jet stream circulation patterns characterized by amplified atmospheric planetary waves that meander around the globe (e.g., Petoukhov et al., 2013; Screen and Simmonds, 2014; Coumou et al., 2014). In particular, it has been found that regional weather is strongly influenced by persistent longitudinal planetary-scale waves with zonal wave numbers 6, 7, or 8 (Petoukhov et al., 2013; Coumou et al., 2014). Under certain conditions, these waves become trapped by midlatitude waveguides and are amplified by a quasi-resonant response to orographic and land-sea thermal forcing (Petoukhov et al., 2013). The quasi-resonant conditions associated with planetary-scale waves, however, require the formation of pertinent waveguides in the zonally averaged flow, and this formation process may involve highly nonlinear dynamics (Palmer, 2013). Nevertheless, the observations in this study were made during the wintertime when a stronger subtropical jet stream (Fig. 1a) acts as a waveguide for the planetary-scale waves.

Therefore, we analyzed the extratropical meridional velocity from the MERRA reanalysis data to characterize the high-amplitude Rossby wave patterns during the observa-

tional period. Even if the amplified Rossby waves with a period of around 8 days are noted previously from Fig. 1, the zonal wave number of Rossby waves are now estimated from the longitudinal distribution of the $v_{200\text{hPa}}$ anomalies over the globe in the extratropical latitudes. Figure 6 shows the power spectrum as a function of zonal wave number estimated based on the FSA using the $v_{200\text{hPa}}$ anomalies shown in Fig. 5a and b. It is apparent from the Fig. 6 that both the spectra show strong power near the zonal wave number 6, further supporting earlier studies. For example, Petoukhov et al. (2013) found the strong contribution of quasi-stationary waves with zonal wave numbers 6, 7 and 8 to several recent severe regional weather extremes. Also, Coumou et al. (2014) demonstrated that the high-amplitude quasi-stationary Rossby waves with zonal wave numbers 6, 7, and 8 resulted in persistent weather conditions at the surface and hence in a midlatitude synchronization of extreme weather, while Teng et al. (2013) showed the heat waves over the United States (US) are affected by the planetary-scale wave number 5. Furthermore, Screen and Simmonds (2014) also demonstrated the link between amplified Rossby waves and surface temperature as well as precipitation extremes in the midlatitudes for the period 1979–2012. From the above studies, it is apparent that the slow-propagating Rossby waves influence the surface weather. Moreover, the slow wave propagation would prolong certain weather conditions and therefore lead to extremes on timescales of weeks. For instance, Fig. 4 shows that the divergence and convergence persists for about 1 week over the observational site, which is further linked with the slow-propagating Rossby waves shown in Fig. 5a and c. Though

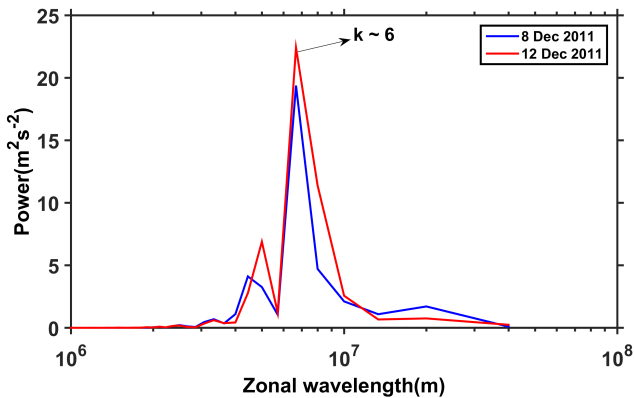


Figure 6. Power spectra of v_{200} hPa anomalies on 8 and 12 December 2011. The spectra are obtained from the Fourier analysis of the longitudinal distribution of v_{200} hPa anomalies over the globe averaged for latitudes between 28–50° N. Both spectra show strong power near the zonal wave number 6.

the propagating Rossby waves on a sub-monthly scale observed in this study do not lead to extreme surface weather conditions, they nevertheless modulate the RH and rainfall patterns and other surface meteorological parameters shown in Fig. 3 considerably.

While the study shows important implications of Rossby waves in relation to surface weather on the timescales of weeks, most of the previous studies discussed above are focused on timescales of over 1 month. The position of the jet stream along with the characteristics of planetary-scale Rossby waves varies substantially from day to day; hence, analysis over longer timescales shows distinct monthly and seasonal patterns. However, more recent studies have investigated the relationship between the sub-monthly predictability and characteristics of Rossby waves, such as their temporal duration, spatial extension, and the area of genesis. For instance, using the 12 000-year integration of an atmospheric general circulation model, Teng et al. (2013) demonstrated that the heat waves over the USA were preceded by 15–20 days by a pattern of planetary-scale waves. Furthermore, Grazzini (2015) reported that the predictive skill increases with the presence of long-period Rossby waves for medium-range forecasts. It is noted that the medium-range forecast skill scores are above average when Rossby waves last for the duration of at least 8 days in the initial conditions. In contrast, bad medium-range forecast skill scores tend to be associated with shorter Rossby wave periods (Grazzini, 2015). In this context, the present study shows the Rossby waves last for at least 8 days in each phase over the study region (see, Fig. 4). Hence, there should be a fair chance of predictability for the timescales of weeks and above.

5 Summary and concluding remarks

In this study, 6-hourly radiosonde observations as well as surface meteorological parameters were analyzed during the GVAX campaign in November–December 2011 at the extratropical site of Manora Peak located in the central Himalayan region. It was observed that the upper-level wind fields were characterized by anomalous high-amplitude Rossby waves with a period of around 8 days. Furthermore, using the global MERRA reanalysis data it was found that the quasi-stationary Rossby waves are characterized by zonal wave number 6. The vertical phase propagation of Rossby waves indicates the downward injection of energy flux from the upper troposphere but with a drastic loss in amplitude due to strong density gradients below the tropopause. However, the propagating Rossby waves established a considerable influence in the surface meteorological parameters. A substantial modulation of Rossby waves is seen in the time series of surface RH and rainfall anomalies. The time series of other surface parameters also fluctuates according to the phase of upper-tropospheric Rossby waves. We further demonstrated the link between the Rossby waves and surface weather by analyzing the MERRA wind field data. The propagating Rossby waves in the upper troposphere along with the undulations in the jet stream create convergence and divergence regions in the mid-troposphere. Moreover, the convergence–divergence couplet modulates the surface meteorological parameters during the observational period.

The characteristics of the planetary-scale waves observed in this study are consistent with those of previous studies. However, the present study further investigates the evolution of the upper-tropospheric circulation anomalies associated with the wet and dry conditions near the surface at the observational site during winter. The winter seasonal anomaly is observed to be associated with several rapidly intensifying and decaying, large-amplitude, anomalous cyclonic and anti-cyclonic circulations. Furthermore, these anomalous circulations in the upper troposphere are linked with the propagating Rossby waves circumnavigating the globe. Hence, the study further implies that the hydrological extremes over the region during the winter can be studied through the succession of events rather than as a single seasonal event. In addition, it can be concluded that improved process understanding and better coordinated modeling and observational studies will be needed to advance the medium-range forecasts over the study region.

Acknowledgements. Ganges Valley Aerosol Experiment (GVAX) was a collaborative effort between the US Department of Energy Atmospheric Radiation Measurement (ARM) Program, the Indian Institute of Science (IISc) and the Indian Space Research Organization (ISRO), and the Aryabhatta Research Institute of Observational Sciences (ARIES). The authors are thankful to the ARM Climate Research Facility for providing the data utilized in the present study (<http://www.archive.arm.gov>). TRMM and MERRA reanaly-

sis data sets used in this effort were acquired as part of the activities of NASA's Science Mission Directorate and are archived and distributed by the Goddard Earth Sciences (GES) Data and Information Services Center (DISC) (<http://mirador.gsfc.nasa.gov/>). We are also thankful to the Global Modeling and Assimilation Office (GMAO) and the GES DISC for the dissemination of MERRA data. D. V. Phanikumar thanks the Director of ARIES for providing the necessary support.

The topical editor, V. Kotroni, thanks R. Kramer and one anonymous referee for help in evaluating this paper.

References

- Branstator, G.: Circum global teleconnections, the jet stream waveguide, and the North Atlantic Oscillation, *J. Climate*, 15, 1893–1910, 2002.
- Chang, E. K. M. and Yu, D. B.: Characteristics of Wave Packets in the Upper Troposphere. Part I: Northern Hemisphere Winter, *J. Atmos. Sci.*, 56, 1708–1728, 1999.
- Chen, P. and Newman, M.: Rossby Wave Propagation and the Rapid Development of Upper-Level Anomalous Anticyclones during the 1988 U.S. Drought, *J. Climate*, 11, 2491–2504, 1998.
- Coumou, D. and Rahmstorf, S.: A decade of weather extremes, *Nature Climate Change*, 2, 491–496, doi:10.1038/nclimate1452, 2012.
- Coumou, D., Petoukhov, V., Rahmstorf, S., Petri, S., and Schellnhuber, H. J.: Quasi-resonant circulation regimes and hemispheric synchronization of extreme weather in boreal summer, *P. Natl. Acad. Sci. USA*, 111, 12331–12336, doi:10.1073/pnas.1412797111, 2014.
- Davies, H. C. and Didone, M.: Diagnosis and dynamics of forecast error growth, *Mon. Weather Rev.*, 141, 2483–2501, 2013.
- Forbes, J. M.: Tidal and Planetary Waves, in: The Upper Mesosphere and Lower Thermosphere: A Review of Experiment and Theory, edited by: Johnson, R. M. and Killeen, T. L., American Geophysical Union, Washington, D.C., USA, doi:10.1029/GM087p0067, 1995.
- Fritsch, J. M. and Carbone, R. E.: Improving Quantitative Precipitation Forecasts in the Warm Season: A USWRP Research and Development Strategy, *B. Am. Meteorol. Soc.*, 85, 955–965, 2004.
- Gómara, I., Pinto, J. G., Woollings, T., Masato, G., Zurita-Gotor, P., and Rodríguez-Fonseca, B.: Rossby wave-breaking analysis of explosive cyclones in the Euro-Atlantic sector, *Q. J. Roy. Meteor. Soc.*, 140, 738–753, doi:10.1002/qj.2190, 2014.
- Goswami, B. N., Venugopal, V., Sengupta, D., Madhusoodanan, M. S., and Xavier, P. K.: Increasing trend of extreme rain events over India in a warming environment, *Science*, 314, 1442–1445, 2006.
- Grazzini, F.: Predictability of a large-scale flow conducive to extreme precipitation over the western Alps, *Meteorol. Atmos. Phys.*, 95, 123–138, 2007.
- Grazzini, F.: Atmospheric predictability and Rossby wave packets, *Q. J. Roy. Meteorol. Soc.*, 141, 2793–2802, doi:10.1002/qj.2564, 2015.
- Grazzini, F. and Van der Grijn, G.: Central European floods during summer 2002, *ECMWF Newsletter*, 18–28, 2003.
- Guhathakurtha, P., Sreejith, O. P., and Menon, P. A.: Impact of climate change on extreme rainfall events and flood risk in India, *J. Earth Syst. Sci.*, 120, 359–373, 2011.
- Hardwick Jones, R., Westra, S., and Sharma, A.: Observed relationships between extreme sub-daily precipitation, surface temperature, and relative humidity, *Geophys. Res. Lett.*, 37, L22805, doi:10.1029/2010GL045081, 2010.
- Hoskins, B.: Predictability of Weather and Climate, chapter: Predictability from a dynamical meteorological perspective, Cambridge University Press, Cambridge, UK, 30–39, 2006.
- Hoskins, B. J. and Ambrizzi, T.: Rossby wave propagation on a realistic longitudinally varying flow, *J. Atmos. Sci.*, 50, 1661–1671, 1993.
- Hoskins, B. J. and Karoly, D. J.: The steady linear response of a spherical atmosphere to thermal and orographic forcing, *J. Atmos. Sci.*, 38, 1179–1196, 1981.
- Huffman, G. J., Bolvin, D. T., Nelkin, E. J., Wolff, D. B., Adler, R. F., Gu, G., Hong, Y., Bowman, K. P., and Stocker, E. F.: The TRMM Multisatellite Precipitation Analysis (TMPA): Quasi-global, multiyear, combined-sensor precipitation estimates at fine scales, *J. Hydrometeorol.*, 8, 38–55, doi:10.1175/JHM560.1, 2007.
- IPCC: Managing the Risks of Extreme Events and Disasters to Advance Climate Change Adaption, edited by: Field, C. B., Barros, V., Stocker, T. F., Qin, D., Dokken, D. J., Ebi, K. L., Mastrandrea, M. D., Mach, K. J., Plattner, G. K., Allen, S. K., Tignor, M., and Midgley, P. M., Cambridge University Press, Cambridge, UK, 109–230, 2012.
- Jenkins, G. W. and Watts, D. G.: Spectral Analysis and its Applications, Holden-Day, San Francisco, CA, USA, 16–54, 1968.
- Joseph, S., Sahai, A. K., Sharmila, S., Abhilash, A., Borah, N., Chattopadhyay, R., Pillai, P. A., Rajeevan, M., and Kumar, A.: North Indian heavy rainfall event during June 2013: diagnostics and extended range prediction, *Clim. Dynam.*, 44, 2049–2065, doi:10.1007/s00382-014-2291-5, 2015.
- Lyon, B. and Dole, R. M.: A Diagnostic Comparison of the 1980 and 1988 U.S. Summer Heat Wave-Droughts, *J. Climate*, 8, 1658–1675, 1995.
- Martius, O., Zenklusen, E., Schwierz, C., and Davies, H. C.: Episodes of Alpine heavy precipitation with an overlying elongated stratospheric intrusion: A climatology, *Int. J. Climatol.*, 26, 1149–1164, 2006.
- Massacand, A. C., Wernli, H., and Davies, H. C.: Influence of upstream diabatic heating upon an alpine event of heavy precipitation, *Mon. Weather Rev.*, 129, 2822–2828, 2001.
- Nibanupudi, H. K., Gupta, A. K., and Rawat, P. K. Mountain Hazards and Disaster Risk: Mitigating Climatic and Human Induced Disaster Risks Through Ecosystem Resilience: Harmonizing Built and Natural Environments in the KKH Region, edited by: Nibanupudi, H. K. and Shaw, R., 139–158, doi:10.1007/978-4-431-55242-0, Springer, Tokyo, Japan, 2015.
- Niranjan Kumar, K. and Ouarda, T. B. M. J.: Precipitation variability over UAE and global SST teleconnections, *J. Geophys. Res.-Atmos.*, 119, 10313–10322, doi:10.1002/2014JD021724, 2014.
- Niranjan Kumar, K., Entekhabi, D., and Molini, A.: Hydrological extremes in hyper-arid regions: A diagnostic characterization of intense precipitation over the Central Arabian Peninsula, *J. Geophys. Res.-Atmos.*, 120, 1637–1650, doi:10.1002/2014JD022341, 2015.
- Palmer, T. N.: Climate extremes and the role of dynamics, *P. Natl. Acad. Sci. USA*, 110, 5281–5282, doi:10.1073/pnas.1303295110, 2013.

- Petoukhov, V., Rahmstorf, S., Petri, S., and Schellnhuber, H. J.: Quasiresonant amplification of planetary waves and recent Northern Hemisphere weather extremes, *P. Natl. Acad. Sci. USA*, 110, 5336–5341, 2013.
- Pielke Jr. R. A. and Klein, R. A.: Extreme Weather Sourcebook 2001 Edition, Environmental and Societal Impacts Group, National Center for Atmospheric Research, and the American Meteorological Society, USA, 2001.
- Press, W. H., Teukolsky, S. A., Vetterling S. T., and Flannery, B. P.: Numerical recipes in C: the art of scientific computing, 2nd edition, Cambridge University Press, Cambridge, UK, 537–608, 1994.
- Rahmstorf, S. and Coumou, D.: Increase of extreme events in a warming world, *P. Natl. Acad. Sci. USA*, 108, 17905–17909, doi:10.1073/pnas.1101766108, 2011.
- Rajeevan, M., Bhate, J., and Jaiswal, A. K.: Analysis of variability and trends of extreme rainfall events over India using 104 years of gridded daily rainfall data, *Geophys. Res. Lett.*, 35, L18707, doi:10.1029/2008GL035143, 2008.
- Rienecker, M. M., Suarez, M. J., Gelaro, R., Todling, R., Bacmeister, J., Liu, E., Bosilovich, M. G., Schubert, S. D., Takacs, L., Kim, G.-K., Bloom, S., Chen, J., Collins, D., Conaty, A., da Silva, A., Gu, W., Joiner, J., Koster, R. D., Lucchesi, R., Molod, A., Owens, T., Pawson, S., Pegion, P., Redder, C. R., Reichle, R., Robertson, F. R., Ruddick, A. G., Sienkiewicz, M., and Woollen, J.: MERRA: NASA's Modern-Era Retrospective Analysis for Research and Applications, *J. Climate*, 24, 3624–3648, doi:10.1175/JCLI-D-11-00015.1, 2011.
- Sardeshmukh, P. D. and Hoskins, B. J.: The generation of global rotational flow by steady idealized tropical divergence, *J. Atmos. Sci.*, 45, 1228–1251, 1988.
- Schubert, S., Wang, H., and Suarez, M.: Warm Season Subseasonal Variability and Climate Extremes in the Northern Hemisphere: The Role of Stationary Rossby Waves, *J. Climate*, 24, 4773–4792, 2011.
- Schwierz, C., Dirren, S., and Davies, H. C.: Forced waves on a zonally aligned jet stream, *J. Atmos. Sci.*, 61, 73–87, 2004a.
- Schwierz, C., Croci-Maspoli, M., and Davies, H. C.: A perspicacious indicator of atmospheric blocking, *Geophys. Res. Lett.*, 31, L06125, doi:10.1029/2003GL019341, 2004b.
- Screen, J. A. and Simmonds, I.: Amplified mid-latitude planetary waves favour particular regional weather extremes, *Nature Climate Change*, 4, 704–709, 2014.
- Shapiro, M. and Thorpe, A.: THORPEX International Science Plan, WMO, WWRP, USA, 2004.
- Sinha Ray, K. C. and Srivastava, A. K.: Is there any change in extreme events like drought and heavy rainfall?, *Curr. Sci. India*, 79, 155–158, 2000.
- Smith, S. W.: The Scientist and Engineer's Guide to Digital Signal Processing, San Diego, CA, California Technical Pub., 243–260, 1997.
- Teng, H., Branstator, G., Wang, H., Meehl, G. A., and Washington, W. M.: Probability of US heat waves affected by a sub-seasonal planetary wave pattern, *Nat. Geosci.*, 6, 1056–1061, doi:10.1038/ngeo1988, 2013.
- Wirth, V. and Eichhorn, J.: Long-lived Rossby wave trains as precursors to strong winter cyclones over Europe, *Q. J. Roy. Meteorol. Soc.*, 140, 729–737, doi:10.1002/qj.2191, 2014.